UNITED STATES DEPARTMENT OF THE INTERIOR

GEOLOGICAL SURVEY

USE OF MULTISPECTRAL SCANNER IMAGES FOR ASSESSMENT OF HYDROTHERMAL ALTERATION IN THE MARYSVALE, UTAH, MINING AREA

By

Melvin H. Podwysocki, Donald B. Segal, Michael J. Abrams

Open-File Report 82-675

Abstract

Multispectral images of an area near Marysvale, Utah, were collected by using the airborne U.S. National Aeronautics and Space Administration (NASA) 24-channel Bendix multispectral scanner; they were analyzed to define areas of hydrothermally altered, potentially mineralized rocks. Hydrothermally altered rocks, particularly volcanic rocks affected by solutions rich in sulfuric acid, are commonly characterized by concentrations of argillic minerals such as alunite and kaolinite. These minerals are important for identifying hydrothermally altered rocks in multispectral images because they have an intense absorption band centered near a wavelength of 2.2 um. Unaltered volcanic rocks commonly lack these minerals and hence do not have the absorption band. Limonitic minerals, such as goethite, hematite, jarosite, and lepidocrocite also are commonly associated with these deposits as a result of primary and secondary processes. However, limonite also is widespread on unaltered rocks and is not abundant on some altered rocks in the study area. Of the minerals mentioned above, alunite is the only mineral in the area studied that is a unique product of hydrothermal processes.

A color-composite image was constructed using the following spectral band ratios: 1.6um/2.2um, 0.67um/1.0um, and 1.6um/0.48um. The 1.6um/2.2um ratio contrasts the 1.6-um region which contains no significant absorption bands against the 2.2-um region to define 1) rocks having an absorption band near 2.2 um indicative of both alunite and kaolinite, and 2) minerals containing large amounts of water in their crystal lattice, such as zeolites, 2:1 layered clays, and gypsum, and vegetation having a high water content in its leaf structure, creating an overall depression of the 2.2-um region due to an intense water absorption band near 2.7 um. A 0.67um/1.0um ratio was used to define vegetated areas on the basis of a chlorophyll absorption band centered in the 0.4-0.7-um region and the lack of absorption in the 1.0-um region. The 1.6um/0.48um ratio was chosen to detect limonitic minerals, which have a broad ferric-iron absorption band centered in the ultraviolet region. This color-ratio composite image was successfully used to distinguish several types of hydrothermally altered rocks from unaltered rocks and rocks from vegetation.

The individual gray levels in a black and white image of the 1.6um/2.2um ratio were assigned to specific colors. This color image, known as a color-coded density slice, depicts the varying levels of absorption in the 2.2-um region caused by the above-mentioned phenomena. Thus, vegetation tends to show the same range of colors in the density slice as do hydrothermally altered rocks.

A black-and-white transparency of the 0.67um/1.0um ratio, which shows vegetation as black to dark gray, when overlayed on the 1.6um/2.2um color-coded ratio image, effectively masked out those areas covered by vegetation, thereby eliminating the vegetation-rock ambiguity. By accentuating rocks containing varying amounts of alunite and kaolinite, the combined mask and density slice more graphically define the hydrothermally altered areas than does the color-ratio composite image and also reveals a zonation within the altered areas. The most intense absorption shows many details of the paleohydrothermal cells responsible for the alteration.

Use of color-ratio composite images and color-coded density slicing in conjunction with masking is an effective means of defining the distribution of hydrothermal alteration products. These techniques use scanner bands that are

equivalents of those in the Thematic Mapper, a multispectral scanner to be launched on the Landsat-D satellite in 1982. These techniques, along with the Thematic Mapper bands, should provide a rapid and more accurate means of defining hydrothermally altered areas than is possible by using the present Landsat multispectral scanner data.

Introduction

The Marysvale, Utah, area is located within a large volcanic field, and at many localities, the volcanic rocks have been altered by acidic hydrothermal solutions. Some of these altered areas contain economic mineral deposits that have sparked several mining booms in the region. Precious metals were exploited in the 1800's, alunite during World Wars I and II, and uranium from the late 1940's to the 1960's. Cunningham and Steven (1979) have suggested that a potential for buried porphyry molybdenum deposits exists in this region.

This paper describes some preliminary analytical results obtained utilizing aircraft multispectral scanner images for the detection of hydrothermally altered rocks in the Marysvale region. The techniques use bands in the visible and near-infrared portion of the electromagnetic spectrum that approximate those of the Thematic Mapper multispectral scanner scheduled for launch on the Landsat-D satellite in 1982. Results indicate the techniques can: 1) distinguish readily between altered and unaltered volcanic rocks, 2) recognize areas of hydrothermally altered rocks not previously mapped, and 3) distinguish different types of altered rocks.

Physical Setting

Marysvale is located approximately 260 km south of Salt Lake City, Utah. The nearby study area (fig. 1) lies within the High Plateaus of Utah subprovince of the Colorado Plateaus province, a transition zone between relatively flatlying rocks to the east and the blockfaulted rocks of the Basin and Range province to the west. Altitudes within the study area range from 2,770 to 1,770 m (approximately 9,100 to 5,800 ft.) above sea level. Topography is moderately rugged; local relief in the western part of the study area exceeds 300 m (1000 ft). In general, altitudes and relief decrease toward the east.

Vegetation is to a high degree related to the topography; higher elevations are occupied by a dense to moderate cover of ponderosa pine (Pinus ponderosa), mountain mahogany (Cercocarpus sp.) and small patches of Gambel oak (Quercus gambelii), bigtooth maple (Acer grandidentatum), and quaking aspen (Populus tremuloides). Lush grasses grow in the mountain meadows. These species are found chiefly in the western third, and to a lesser degree, along the easternmost margin of the study area. Intermediate elevations are overlain by a dense to thin cover of pinyon pine (Pinus edulis) and Utah juniper (Juniperus osteosperma). These species are most common in the central part and less common in the eastern part of the study area. The lower elevations are occupied by a moderate to thin cover of big sagebrush (Artemisia tridentata) and rabbitbrush (Chrysothamnus sp.). These species predominate in the Sevier River canyon and the lower slopes and valley bottoms of the eastern part of the study area. Valleys containing perennial streams also contain some stands of narrowleaf and Fremont cottonwood trees (Populus angustifolia and P. fremontii, respectively).

A simplified geologic map of the study area (fig. 2) shows that Pre-Tertiary rocks are relatively scarce, consisting of several outcrops of Permian Toroweap Formation and Triassic-Jurassic Navajo Sandstone. The Bullion Canyon Volcanics (Callaghan, 1939; Steven, 1978) of Oligocene and Miocene age were extruded 35(?) million to 21 million years ago and unconformably overlie the Paleozoic and Mesozoic sedimentary rocks here and elsewhere in the Marysvale area. The Bullion Canyon consists of intermediate-composition lava flows, volcanic breccias, and ash-flow tuffs that formed local stratovolcanoes (Cunningham and Steven, 1979). About 23 million years ago, the Bullion Canyon was intruded by quartz monzonite stocks, which created convection cells of hydrothermal waters in adjacent wall rocks. The alunite and kaolinite deposits presently exposed within the study area formed near the upwelling cores of these cells (Cunningham and Steven, 1979). The Monroe Peak caldera, located mostly east of the study area, was active about 22 million years ago; related quartz monzonite intrusive and rhyodacite extrusive rocks extend into the eastern part of the study area. About 21 million years ago, the composition of the volcanic rocks erupted (the Mount Belknap Volcanics) became more silicic. Two source areas for the Mount Belknap rocks are indicated: the widespread Joe Lott Tuff Member originated from the Mount Belknap caldera in the Tushar Mountains west of the study area about 19 million years ago; the other units of the Mount Belknap, including rhyolitic ash-flow tuffs, domes and volcanic flows, and granitic intrusive rocks, were

derived from local sources within the study area. Mount Belknap Volcanics continued to be emplaced until at least 14 million years ago (Cunningham and Steven, 1979). These rocks are believed to have originated from a series of shallow cupolas that extended upward from a deeper undifferentiated magma (Cunningham and Steven, 1979). The volcanic sequence is capped in places by locally derived fine-grained water-laid sediments of the Sevier River Formation of Miocene and Pliocene age. Quaternary alluvium, travertine, and landslide materials cover bedrock in large parts of the study area.

Data Processing and Analysis

The multispectral scanner data were collected with the Bendix[1] 24-channel scanner developed for the U.S. National Aeronautical & Space Administration (NASA) and flown on NASA'S NC-130 Hercules aircraft on June 15, 1976, at approximately 12:50 p.m. Mountain Standard Time. Ground resolution is approximately 8-10 m. Although the scanner was configured for 24 channels of data covering the range of 0.34 to 13.0 um, only those channels from 0.34 to 4.75 um were operational for this flight. Furthermore, only five specific channels from those available were chosen for presentation in this paper. Their channel numbers and bandwidths are given in Table 1; and the reasoning to support their use is given in subsequent sections of this paper.

1/ Any use of trade names in this report is for descriptive purposes and does not constitute endorsement by the U.S. Geological Survey.

The multispectral data were used to differentiate hydrothermally altered rocks from all other materials. Band ratioing was used to enhance spectral contrasts to achieve this goal. A discussion of some of the spectra presented in figure 3 will illustrate the reasons for the above choice of bands and the rationale for the use of band ratios.

Two approaches are possible for the selection of bands to distinguish between various types of materials. One method involves a statistical approach, wherein a group of variables (bands or their ratios) and a set of two or more types of materials to be distinguished are categorized a priori (i.e., altered rocks versus unaltered rocks or all rocks versus vegetation). Linear discriminant analysis (Davis, 1973) is one such technique and is well directed toward problems where differences between materials are relatively small, thus requiring a stochastic approach (Conel and others, 1978). Rowan and Kahle (1982) have used such a method to demonstrate that the bands chosen for this study are suitable for distinguishing between unaltered and hydrothermally altered rocks.

However, when contrasts are as strong as those in the rocks dealt with in this study, we believe that a heuristic approach involving examination of the spectral response curves of rocks and vegetation is sufficient in the definition of the bands and their ratios required to achieve our goal. Thus, the more rigorous statistical approach is not needed.

Representative spectral-reflectance data in the region from 0.4 to 2.5 um were obtained for some selected rocks and plant species found in the study area (fig. 3). The data were collected using the NASA - Jet Propulsion Lab's Portable Field Reflectance Spectrometer (PFRS) (Goetz and others, 1975). The vegetation spectra have been taken from Milton (1978), and the rock spectra were collected during this study. No data were collected between 1.3-1.5 and 1.75-2.0 um because of the severe absorption caused by atmospheric water for these portions of the spectrum.

Vegetation (spectra 7, 8, and 9, fig. 3) offers some of the sharpest contrasts in its spectral response. Reflectance is generally low in the visible part of the spectrum because of absorption by plant pigments and is high in the near infrared because of internal leaf scattering and lack of absorption by chlorophyll and water (Knipling, 1970). The relative low reflectance of vegetation beyond 1.3 um is caused by the overwhelming absorption due to water in the leaf structures (Gates and others, 1965; Knipling, 1970).

Several distinctive broad-banded absorption features due to electronic processes within the crystal lattices of minerals can be seen in the rock spectra between 0.4 and 1.0 um. Minerals displaying these absorption features include goethite, hematite, jarosite, and lepidocrocite, among others (Hunt and others, 1971). Limonite often is used as a general field term to describe these minerals and their mixtures (Blanchard, 1968) and will be used here in referring to these minerals. One of the strongest of the absorption features is the marked falloff in reflectance from 0.7 to 0.4 um (spectra 3, 4, 5, and 6, fig. 3), which is associated with a ferric iron absorption band centered in the near ultraviolet region below 0.4 um (Hunt and others, 1971; Hunt and Ashley, 1979). Another absorption band depicted as a shoulder in the spectral curve of goethite occurs at 0.65 um (spectral curve 6, fig. 3). Relatively broad but shallow absorption bands also occur at 0.85 um for hematite and at 0.93 um (spectra 4, 5 and 6, fig. 3) for goethite and other limonitic minerals (Hunt and others, 1971; Hunt and Ashley, 1979).

A set of distinctive narrow-band absorption features caused by vibrational processes within mineral lattice structures can also be observed in the rock spectra (Hunt and Ashley, 1979). These features are found at longer wavelengths, between 1.3-1.5, 1.75-1.95 and 2.10-2.35 um. Minerals commonly found in hydrothermally altered rocks, such as pyrophyllite, sericite, alunite, kaolinite, montmorillonite, and jarosite, may be recognized by absorption bands within these ranges (Hunt, 1979; Hunt and Ashley, 1979). Only the last of these three ranges can be utilized by passive remote sensing systems because the first two bands are in regions where atmospheric water absorbs the incoming solar energy. The absorption bands in the 2.10-2.35-um region are overtones of Al-O-H absorption bands beyond 2.5 um (Hunt, 1981). Because of their unique form and wavelength position, the spectral curves can be utilized to identify several individual minerals (Hunt, 1979).

Unfortunately, for most minerals, very high spectral resolution, on the order of 0.01 um, is required to make unique identifications; absorption bands in the regions made opaque by atmospheric water commonly are needed for differentiation. In the 2.2-um region, airborne scanner bandwidths of 0.25 um are necessary because of the limited solar energy reaching the ground in this region. Thus, airborne or satellite-based scanners, for the present, can only detect the presence of absorption bands in this region, but cannot identify the precise mineral. Airborne (Collins and others, 1981) and spaceborne (Goetz and Rowan, 1981; Rowan and others, 1982) spectroradiometers as well as ground-based portable field instruments can fill this gap.

Two obvious examples of absorption bands in the 2.2-um region can be seen in the rock spectra illustrated in figure 3. The distinctive strong absorption associated with the hydrothermal mineral alunite is seen in spectral curve 6 (fig. 3). The band, as depicted in the PFRS data, actually is composed of two absorption minima, centered at 2.17 and 2.20 um with the 2.17-um band being stronger (Hunt, 1979). Because the PFRS is limited by a spectral resoultion of 0.04 um in this wavelength region (Goetz and others, 1975) it is unable to resolve these minima. Rather, one absorption band centered closer to 2.17 um is shown. Kaolinite also has two absorption minima centered at 2.17 and 2.20 um (Hunt, 1979). However, in kaolinite, the 2.20-um band is stronger. Thus, the kaolinite spectrum as depicted in the PFRS data has a subtle shift in the position of the absorption-band minimum toward longer wavelength (spectral curve 4, fig. 3).

Band Ratioing

Band ratioing has been used successfully to enhance the sometimes subtle differences or contrasts in spectral response between the ratioed bands (Rowan and others, 1974). Ratioing also serves to minimize differences in albedo and the orientation of slopes with respect to the illumination source (Rowan and others, 1974). Minimizing the effects of albedo, however, can lead to ambiguities, as illustrated by ratios of reflectance values from some of the spectra in figure 3 (table 2). Ratio values for each material in the table were calculated by graphically determining the mean reflectance values for the respective channel utilized in a ratio using the bandwidths shown on figure 3.

The 6/10 ratio was chosen to contrast the spectra of vegetation against other materials, primarily rocks and soil. Note that because of the relatively low values in channel 6 and high values in channel 10, vegetation will have relatively low ratio values. Conversely, rocks show much less spectral contrast between the two bands; therefore, their ratios approach unity. Ratios can be depicted in image form by scaling the ratio values into image gray levels, black representing the lowest values and white representing the highest values. Thus, vegetation would appear black to dark gray on an image of the 6/10 ratio, whereas nonvegetated areas would appear light gray to white.

The 12/13 ratio was chosen to emphasize the spectral contrasts between the 1.6- and 2.2-um regions. The phenomena expressed in this ratio include: 1) absorption due to specific Al-O-H stretching and bending moments in minerals such as those mentioned earlier; 2) the overall lowering of albedo of a rock because of molecular water in the crystal lattices of the component minerals; 3) the water content of plants. Those materials having low ratio values (unaltered rocks) would appear dark on the image, and those having high ratio values (altered rocks, vegetation, zeolite, shale) would appear light.

Finally, the 12/3 ratio emphasizes the spectral contrast between limonitic and nonlimonitic rocks. Nonlimonitic rocks would appear darker and limonitic rocks and vegetation would appear light gray to white in a 12/3 ratio image.

Note that rocks have an overall high albedo in the region beyond 1.5 um compared with that of vegetation, but that this distinction is lost by band ratioing. For example, compare the similarity between the 12/3 ratio values for the orange hydrothermally altered latite, white zeolite, and the bigtooth maple (table 2 and fig. 3, spectra 6, 2 and 7, respectively). Although the white zeolite and orange rock are readily distinguished, the orange rock and maple have relatively similar ratio values. Neither the orange altered rock nor the white zeolite are readily distinguishable from the bigtooth maple in the 12/13 ratio. However, the 6/10 ratio is distinctly different, so that both the orange rock and zeolite can be distinguished from the maple in this ratio. More will be said of these differentiations in later paragraphs.

A color-ratio composite (CRC) image (fig. 4) can be constructed using the gray levels of the individual ratios to modulate the intensity of the three additive primary colors. This can be done in a color-additive viewer or a color-film recorder that displays the 12/13 ratio as red, the 6/10 ratio as green and the 12/3 ratio as blue. Refer to figure 5 for a schematic representation of the resultant colors derived from color-additive viewing.

Argillic rocks (or those containing large amounts of molecular water in their mineral lattices) lacking limonite will have relatively high 6/10 and 12/13 ratios and a low 12/3 ratio. The resultant strong red and green components will produce yellow (See table 3). Argillic rocks that contain limonite have a high 12/3 ratio in addition to high 12/13 and 6/10 ratios. Therefore, the three colors of equally high value will produce white. Limonitic rocks lacking a significant argillic content will have a low to medium 12/13 ratio and high 12/3 and 6/10 ratios, resulting in a small red and large blue and green components, producing light blue. Those rocks that are spectrally flat (no limonite or hydroxyl absorption bands) will have relatively high 6/10 and low 12/3 and 12/13 ratio values. The resultant additive color will be high in green and low in red and blue, producing green on the color composite.

Vegetation may yield several different colors on the CRC. Pinyon pine and Utah juniper, which have similar spectra, have a low 6/10 ratio because of chlorophyll absorption and high 12/3 and 12/13 values because of the effects of chlorophyll and water, respectively. The resultant low-intensity green and medium- to high-intensity red and blue components yield magenta. Sagebrush growing in conditions found on the lower slopes of valley walls and on dry valley flats is characterized by low to medium 6/10 and 12/13 ratios and a medium to high 12/3 ratio. This produces low- to medium-intensity green and red components and a high blue component, resulting in dark blue. Vegetation that has lost its chlorophyll absorption but still contains considerable water will display a low 12/3, medium 6/10 and high 12/13 ratios. Grasses and grain crops which turn yellow on maturity characteristically have such spectra. The resultant color combination from these ratio loadings will be red to orange. The very dark areas, shown as nearly black on the CRC, are occupied by less dense cover of pinyon pine and juniper. This color, which results from low values in all three ratios, appears to be a product of a mixing of vegetation and rock spectra.

Examination of the CRC image (fig. 4) reveals many areas of potential interest to the exploration geologist. Those areas shown as yellow (interpreted as argillic) and white (interpreted as limonitic and argillic) correspond well to areas of hydrothermally altered rocks, as noted on the geologic map (compare figs. 2 and 4). Most of the altered rocks are contained within the Bullion Canyon volcanic units. Cunningham (pers. comm., 1981) has confirmed that alunite dated from the altered volcanic rocks yields dates of about 23 million years and that the alunite was formed in near-surface environments during the emplacement of the 23-million-year-old quartz monzonite Central Intrusive. Comparison of the alteration noted on the geologic map and the image mosaic reveals that the area of the Iron Hat (A, fig. 4) is not characterized by the strong yellow or white colors. Detailed field mapping (C. G. Cunningham, pers. comm., 1981) has revealed that the overall pattern of alteration here formed a vertically zoned sequence of rocks in which a highly argillized zone is overlain in turn by a hematite-rich, weakly argillized zone (light blue on the CRC) capped by a highly silicified hematitic rock that masks the underlying argillic zone. Conversely, several areas on the CRC that bear colors indicating hydrothermally altered rocks are not noted on the geologic map. Area B on figure 4, shown primarily as light blue (limonitic) with some white (limonitic and argillic), and yellow (argillic), coincides with the uranium-producing Central Mining Area. Mineralization in this area was confined chiefly to fractures in the fine-grained granitic rocks of the Mount Belknap Volcanics, the 23-million-year-old

quartz monzonite Central Intrusive, or the older Bullion Canyon Volcanics. Mineralizing solutions were fluorine-rich, and sulfur-poor; hence, argillic minerals are not common (Steven and others, 1980). The lack of argillized rocks most likely prompted the mappers not to include the Central Mining Area in the altered category; however, enough alteration is present to be detected by the scanner. Area C is an altered area that had been missed in the field mapping; field examination has revealed altered rocks analogous to those at Big Rock Candy Mountain, approximately 2 km to the southeast.

The white and yellow areas shown on figure 4 at D and E depict areas where the basal portion of the Joe Lott Tuff Member of the Mount Belknap Volcanics has been altered diagenetically to the zeolite mineral clinoptilolite, which formed shortly after emplacement of the tuffs by interaction of water with the still hot ashfall tuffs.

Because zeolites have a high water content within their lattice structures, their reflectance spectra are depressed throughout the 2.1-2.5-um region. Hence, because of the relatively broad bandwidth of the scanner channel in the 2.2-um region, the zeolites yield 1.6um/2.2um ratios similar to those for argillized rocks and therefore are undistinguishable from the argillized rocks on the CRC image.

Although the bands and band ratios were chosen to contrast hydrothermally altered rocks against other materials, some mapping of geologic units other than altered rocks is possible. The Joe Lott Tuff Member of the Mount Belknap Volcanics, where not altered to zeolitic rocks, is shown in light to dark blue on the CRC (G, fig. 4) attesting to its light tan color and some growth of sagebrush. A dacite dome mapped as part of the volcanic rocks of the Monroe Peak caldera (H, fig. 4) appears nearly black on the CRC. The color most probably is related to the generally flat spectral response of these dark rocks and to their light cover of pinyon pine, Utah juniper, and sage. Other combinations of bands and/or band ratios in conjunction with image enhancement or classification procedures probably would allow mapping of other geologic units.

Density slicing and masking

Density slicing is a digital procedure by which individual gray levels or groups of gray levels in a black and white image may be assigned arbitrarily chosen colors. Thus, colors in a density slice-image can be related to specific gray levels and their related digital numbers. Unlike standard color compositing such as a CRC, which uses three channels of data, a density slice may be performed on only a single channel of data.

Ashley and Abrams (1980) have shown that density slicing may be applied to the 12/13 ratio and that individual levels in the density slice can be related to estimates of hydroxyl content in the rocks. Inspection of the 12/13 ratio values for the PFRS data (table 2) shows that the argillically altered orange latite does have the highest ratio for rocks and that zeolite and unaltered rhyolite have respectively lower ratios. Therefore, density slicing of the 12/13 ratio ought to depict differences in the image that might not otherwise be separated in the colors chosen for the CRC image. Note however, that vegetation gives equally high or higher 12/13 ratio values, and it would be difficult, if not impossible, to distinguish hydroxyl-bearing rocks from vegetation solely on the basis of the 12/13 ratio image.

The density slice method may still be used to depict absorption by rock materials at 2.2 um by utilizing a photographic masking technique described by Segal and Podwysocki (1980). In short, if a black and white transparency can be produced on which an undesired type of information is shown as black, that transparency will mask out undesired data when overlaid on other images of the same area. Thus, to mask out those high 12/13 ratio values associated with vegetation, a black and white transparency of the 6/10 ratio can be used. As noted previously, vegetation has a relatively low 6/10 ratio (see fig. 3 and table 2) and appears dark in the image. When suitably duplicated onto a black diazo transparency, the heavily vegetated areas can be rendered black on the high-contrast diazo film. Figure 6 illustrates the results of the masking of the 12/13 ratio density slice with the 6/10 ratio vegetation mask. Those areas depicted in black are either rocks having very little 2.2-um absorption relative to 1.6 um or vegetation having a relatively low 0.67-um reflectance relative to 1.0 um.

Because the exact contrast enhancements applied to the ratio data to allow reproduction on film are known, the colors of the density slice can be related to actual ratio values. The ratio values associated with the colors of the density slice range from <0.739 for black to > 1.123 for white (See table 4 for complete color and ratio assignments). These ratio values are considerably less than those calculated from the PFRS data. As an example, the tan soil on the unaltered rhyolite (5, fig. 3 and table 2) has a PFRS ratio value for 1.6um/2.2um ratio of 1.11. The area of the rhyolite on the density slice is depicted as a light green color, which is equivalent to an aircraft scanner ratio value of 0.867-0.893. An area of altered hematitic rocks containing primarily alunite has a PFRS ratio of 1.29. The red color of this area on the density-slice image is equivalent to a ratio value in the range of 1.047-1.072. Further work will be necessary to relate the PFRS ratio values accurately and precisely to those determined from the aircraft scanner. Because of these discrepancies, further discussion will be limited to relating the colors for the density slice to the rock types.

The masked density slice (fig. 6) permits additional discrimination and zonation of the hydrothermally altered rocks compared with that done by using the CRC image (fig. 4). The Iron Hat area (A, figs. 4 and 6) contains little material that has strong 2.2-um absorption. The CRC image shows little white or yellow (A, fig. 4), and the density slice shows primarily as green with some yellow and orange (A, fig. 6). The Central Mining Area, which contains more white on the CRC image (B, fig. 4), contains some green but mainly yellow, and a few scattered orange and to red pixels (the smallest resolved image element of the multispectral scanner), indicating a stronger 2.2-um absorption than that shown by the Iron Hat area. Note that many of the small patches of altered area immediately east and southeast of the Central Mining Area appear to be isolated along fault zones, where increased porosity and permeability may have allowed easier access to mineralizing fluids (fig. 7). Area C (figs. 4 and 6), a previously unrecognized area of altered rocks analogous to that at Big Rock Candy Mountain, stands out in the density slice primarily as white pixels, an indication of the most intense absorption. Those areas underlain by zeolites, which are yellow or white on the CRC image (D and E, fig. 4) and which can be confused with true hydrothermally altered rocks, stand out as shades of yellow to magenta, with only a few pixels showing as white on the masked density slice (D and E, fig. 6). Thus the density slice separates true hydrothermally altered areas, such as Big Rock Candy Mountain or area C, from the zeolites.

These images can also be used in conjunction with field studies for inferring spatial and temporal relationships. For example, an unaltered rhyolite plug related to the Mount Belknap Volcanics cuts the older altered Bullion Canyon Volcanics (F, figs. 4 and 6). The inference by image interpretation is that the alteration took place before the intrusion by the the rhyolite.

The overall pattern shown by the most intensely altered rocks (orange through white, fig. 6) on the density-slice image is especially striking. Field mapping and radiometric dating within the study area and to the south suggest that the most intensely altered rocks in this area are associated with the 23-million-year-old quartz monzonite intrusive rocks in the Bullion Canyon Volcanics (C.G. Cunningham and T. A. Steven, pers. comm., 1981). Heat generated by these intrusive rocks set into motion convective cells of hydrothermal waters, which near the surface created extensive argillized areas by acid sulfate alteration. Thus, Big Rock Candy Mountain (region 1, figs. 4 and 6), the area immediately to the north, east and south of Iron Hat (region 2, figs. 4 and 6) and the large patch of altered rocks about 3 km east-southeast of Iron Hat (region 3, figs. 4 and 6) represent the remnants of three of the paleohydrothermal cells. These and other cells south of the study area form a peripheral halo of altered rocks 8 km wide just outside the Central Intrusive (T. A. Steven and C. G. Cunningham, pers. comm., 1981).

Summary and Conclusions

Digitally processed images of the Marysvale, Utah, area derived from an airborne multispectral scanner were used to define areas of hydrothermally altered rocks. The scanner channels were processed using band ratioing to enhance spectral differences caused by absorption features in the spectra of naturally occurring materials.

Vegetation was detected by use of a 0.67um/1.0um band ratio (channels 6/10), which emphasized the chlorophyll absorption below 0.67 um and the lack of that absorption at 1.0 um. Limonitic rocks and vegetation were sensed by using a 1.6um/0.48um band ratio (channels 12/3). The 0.48-um band sensed the rather broad trivalent iron-absorption band, which occurs at wavelengths less than 0.40 um, and the 1.6-um band acts as a standard band where no absorption occurs. Rocks containing hydroxyl-bearing or zeolitic minerals and vegetation were detected by the 1.6um/2.2um ratio (channels 12/13). Hydroxyl-rich minerals owe their distinctively high ratio values to absorption by specific Al-O-H bonds, whereas the high ratios associated with zeolites and vegetation are caused by water bound within their respective structures.

Combining the three ratios into a color-ratio composite allowed the separation of altered rocks from unaltered rocks and the separation of both types of rocks from vegetation. Some previously unmapped altered areas were found.

A color-coded density slice of the 12/13 ratio overlain by a black and white transparency of the 6/10 ratio to mask out vegetation separated several types of altered rocks. The color levels of the density slice were assignable to rocks containing varying intensities of hydrothermal alteration through the use of ground-based measurements made by a portable field reflectance spectrometer. Unaltered rocks showed 12/13 aircraft scanner ratio values ranging from <0.739 to <0.944; these values are depicted as colors ranging from black to yellow green on the density slice. The slightly altered rocks of the Central Mining Area had aircraft ratio values of 0.944 to <1.021, which are depicted as yellow through orange. Zeolites were characterized by aircraft-scanner ratio values ranging chiefly from 1.021 to ≤ 1.23 (red-orange through magenta), with a few areas having values >1.123 (white). The intensely altered areas have ratio values >1.123.

The results of this study show that the 1.6- and 2.2-um bands provide valuable information useful in mineral exploration. The worldwide application of these bands and techniques via satellite remote sensing should provide the mineral explorationist with a quantum leap in reconnaissance and detailed field-mapping capabilities.

Acknowledgements

We wish to thank the Goddard Space Flight Center of NASA for making the digital aircraft scanner data available. Special thanks go to Richard Machida of Jet Propulsion Laboratories for his work with the Portable Field Reflectance Spectrometer. Lastly, we gratefully acknowledge the invaluable time and assistance, both in the lab and field, provided by Thomas A. Steven and Charles G. Cunningham of the U.S. Geological Survey. Without their help, this study could not have been accomplished.

References

Ashley, R. P., and Abrams, M. J., 1980, Alteration mapping using multispectral images - Cuprite mining district, Esmeralda County, Nevada: U. S. Geological Survey Open-File Report 80-367, 17 p.

Blanchard, Rollin, 1968, Interpretation of leached outcrops: Nevada Bureau of Mines Bulletin 66, 196 p.

Callaghan, Eugene, 1939, Volcanic sequence in the Marysvale region in southwest - central Utah: American Geophysical Union Transactions, v. 20, part 3, p. 438-452.

Collins, W., Chang, S., Kuo, J. T., and Rowan, L. C., 1981, Remote meneralogical analysis using a high-resolution airborne spectro-radiometer: Preliminary results of the Mark II system: Institute of Electrical and Electronic Engineers, 1981 International Geoscience and Remote Sensing Symposium Digest, v. 1, p. 337-344.

Conel, J. E., Abrams, M. J., and Goetz, A. F. H., 1978, A study of alteration associated with uranium occurrences in sandstone and its detection by remote sensing methods: U.S. National Aeronautics and Space Administration, Jet Propulsion Laboratory Publication 78-66, Vols. 1 & 2, 398 p.

Cunningham, C. G., and Steven, T. A., 1979, Uranium in the central mining area, Marysvale district, west central Utah: U.S. Geological Survey Miscellaneous Investigation Series Map I-1177, scale 1:24,000

Cunningham, C. G., Steven, T. A., Rowley, P. D., Glassgold, L. B., and Anderson, J. J., 1981, Preliminary geologic map including argillic and advanced argillic alteration and principal hydrothermal quartz and alunite veins in the Tushar Mountains and adjoining areas, Marysvale volcanic field, Utah: U.S. Geological Survey Open-File Report 81-831, scale 1:50,000.

Davis, J. C., 1973, Statistics and data analysis in geology: New York, John Wiley and Sons, 550 p.

Gates, D. M., Keegan, H. J., Schleter, J. C., and Weidner, V. R., 1965, Spectral properties of plants: Applied Optics, v. 4, no. 1, p. 11-20.

Goetz, A. F. H., Billingsley, F. C., Gillespie, A. R., Abrams, M. J., Squires, R. L., Shoemaker, E. M., Lucchitta, I., and Elston, D. P., 1975, Application of ERTS images and image processing to regional geologic problems and geologic mapping in northern Arizona: U.S. National Aeronautics and Space Administration, Jet Propulsion Laboratory Technical Report 32-1597, 188 p.

Goetz, A. F. H., and Rowan, L. C., 1981, Narrow-band radiometry for minerail identification: Shuttle Multispectral Infrared Radiometer (SMIRR) aircraft test results: Institute of Electrical and Electronic Engineers, 1981 International Geocience and Remote Sensing Symposium Digest, v. 1, p. 345-346.

Hunt, G. R., 1979, Near-infrared (1.3-2.4 um) spectra of alteration minerals - Potential for use in remote sensing: Geophysics, v. 44, no. 12, p. 1974-1986.

Hunt, G. R., 1981, Identification of kaolins and associated minerals in altered volcanic rocks by infrared spectroscopy: Clays and Clay Minerals, v. 29, p. 76-78.

Hunt, G. R., and Ashley, R. P., 1979, Spectra of altered rocks in the visible and near infrared: Economic Geology, v. 74, p. 1613-1629.

Hunt, G. R., Salisbury, J. W., and Lenhoff, D. J., 1971, Visible and near-infrared spectra of minerals and rocks - III Oxides and hydroxides: Modern Geology, v. 2, p. 195-205.

Knipling, E. B., 1970, Physical and physiological basis for the reflectance of visible and near-infrared radiation from vegetation: Remote Sensing of the Environment, v. 1, no. 3, p. 155-159.

Milton, Nancy, 1978, Spectral reflectance measurements of plants in the East Tintic Mountains, Utah: U.S. Geological Survey Open-File Report 78-448, 117 p.

Rowan, L. C., Goetz, A. F. H., and Kingston, M. J., 1982, Spectral radiometry of the Earth: Preliminary results from the Shuttle Multispectral Infrared Radiometer: paper presented at XXIV Committee on Space Research (COSPAR) Conference, Ottawa, Canda, May, 1982.

Rowan, L. C., and Kahle, A. B., 1982, Evaluation of 0.46- to 2.36-micrometer multispectral scanner images of the East Tintic mining district, Utah, for mapping hydrothermally altered rocks: Economic Geology, v. 77, no. 2, p. 441-452.

Rowan, L. C., Wetlaufer, P. H., Goetz, A. F. H., Billingsley, F. C., and Stewart, J. H., 1974, Discrimination of rock types and detection of hydrothermally altered area in south central Nevada by the use of computer-enhanced ERTS images: U.S. Geolgical Survey Professional Paper 883, 35 p.

Segal, D. B., and Podwysocki, M. H., 1980, A technique using diazo film for isolating areas of spectral similarity: U.S. Geological Survey Open-File Report 80-1267, 15 p.

Steven, T. A., 1978, Geologic map of the Sevier SW quadrangle, west-central Utah: U.S. Geological Survey Miscellaneous Field Studies Map MF-962, scale 1:24,000.

Steven, T. A., Cunningham, C. G., and Machette, M. N., 1980, Integrated uranium systems in the Marysvale volcanic field, west-central Utah: U.S. Geological Survey Open-File Report 80-524, 39 p.

Table 1

Channels used in this study and their associated bandwidths

Channel No.	Bandwidths (in um)
3	0.47 - 0.51
6	0.65 - 0.69
10	0.97 - 1.04
12	1.53 - 1.67
13	2.12 - 2.39

Table 2

Band ratios calculated for some representative materials

Material	Band Ratio 6/10	Band Ratio 12/3	Band Ratio 12/13
White zeolite (clinoptilolite)(2)*	0.88	2.03	1.33
Tan Moenkopi Shale (4)	0.88	3.17	1.33
Orange altered latite (6)	0.85	3.53	1.47
Tan soil on unaltered rhyolite (5)	0.89	1.86	1.11
Singleleaf pinyon (8)	0.18	2.00	2.00
Bigtooth maple (7)	0.20	3.67	1.38
Big sagebrush (9)	0.43	3.42	1.37

*Number indicates spectral curve in figure 3.

Table 3

Summary of relationships between color in the CRC image, ratio, color filter and main absorption features. Relative ratio values L = low, M = moderate, and H = High.

Spectral band ratio and filter color				
0.67um/1.0um (green)	1.6um/0.48um (blue)	1.6um/2.2um (red)	Resultant image color	Absorption feature
M-H	L	L	green	None, spectrally flat
H	L	H	yellow	OH^{-1}
H	H	H	white	OH^{-1}, Fe^{+3}
H	H	L-M	blue (light)	Fe^{+3}
L-M	M-H	L-M	blue (dark)	Chlorophyll (moderate) H_2O (moderate)
L	M-H	M-H	magenta	H_2O (intense)
M	L	H	red-orange	Chlorophyll (weak) (H_2O intense)

Table 4

Relationship between density-slice color assignments and 12/13 ratios

Wedge step	Color	Aircraft ratio values
1	Black	<0.739
2	Dark Blue	0.739 to <0.765
3	Medium Blue	0.765 to <0.790
4	Cyan	0.790 to <0.816
5	Cyan-Green	0.816 to <0.842
6	Green	0.842 to <0.867
7	Light Green	0.867 to <0.893
8	Green-Yellow	0.893 to <0.918
9	Yellow-Green	0.918 to <0.944
10	Yellow	0.944 to <0.970
11	Yellow-Orange	0.970 to <0.995
12	Orange	0.995 to <1.021
13	Red-Orange	1.021 to <1.047
14	Red	1.047 to <1.072
15-16	Magenta	1.072 to <1.123
17	White	≥1.123

Figure 1. Location map of the study area. The hachured area depicts the area covered in figure 7.

Figure 2. Generalized geologic map of the study area, showing previously mapped alteration (adapted from Cunningham and others, 1981).

Figure 3. Field spectra gathered by the NASA - Jet Propulsion Lab's Portable Field Reflectance Spectrometer. Reflectances are calculated against a Fiberfrax standard. Numbers and the associated brackets within the graph define the channel numbers and bandwidths of the Bendix multispectral scanner used in this paper. Vegetation spectra are from Milton (1978). The small absorption band located at approximately 1.15 um in spectra 1-4 and 6 is caused by atmospheric water.

Figure 4. Color-ratio composite (CRC) image of the study area. Because of the inherent distortions in airborne scanner data and the length of the flightlines, the data were digitally processed in three segments, each being geometrically corrected to the 1:24000 base map by fifth-order polynomial equations (rubber sheeting). Displacement errors average about 12 m. The three individual segments then were joined together by photomosaicking. See text for explanation of symbols. The numeric annotation on the image refers to overall areas of hydrothermally altered rocks, whereas the alphabetic characters point to specific details within the image.

Figure 5. A triangular diagram representing the endmember colors in color additive space and the band ratios associated with these colors in the CRC image. Along the edges of the triangle, equal amounts of red + blue = magenta, red + green = yellow, and blue + green = cyan. Equal amounts of red + blue + green = white, lack of all three colors = black

Figure 6. Density slice of the 12/13 ratio image overlain by a vegetation mask created from the 6/10 ratio. Color assignments for the density slice begin with black for the lowest ratio images, progressing through lighter shades of blue into green, yellow, orange, red, magenta, and ultimately white for the highest ratio values. Refer to table 4 for further detail. Because of the effect of the black masking, the very lowest 12/13 ratio values (black) will be indistinguishable from the masking effect of the 6/10 ratio. Geometric corrections and annotation are the same as those applied to figure 4.

Figure 7. Map showing the relationship of faulting (modified from Cunningham and others, 1981) to hydrothermal alteration for a part of the Central Mining Area as interpreted from Area B of figure 6. Refer to figure 1 for exact location within the study area. Irregular black patches are areas interpreted from the masked density slice (fig. 6) as having 12/13 aircraft scanner ratio values >0.970 (yellow-orange through white colors). Note aligned patches of alteration that may be additional faults not recognized in the field.

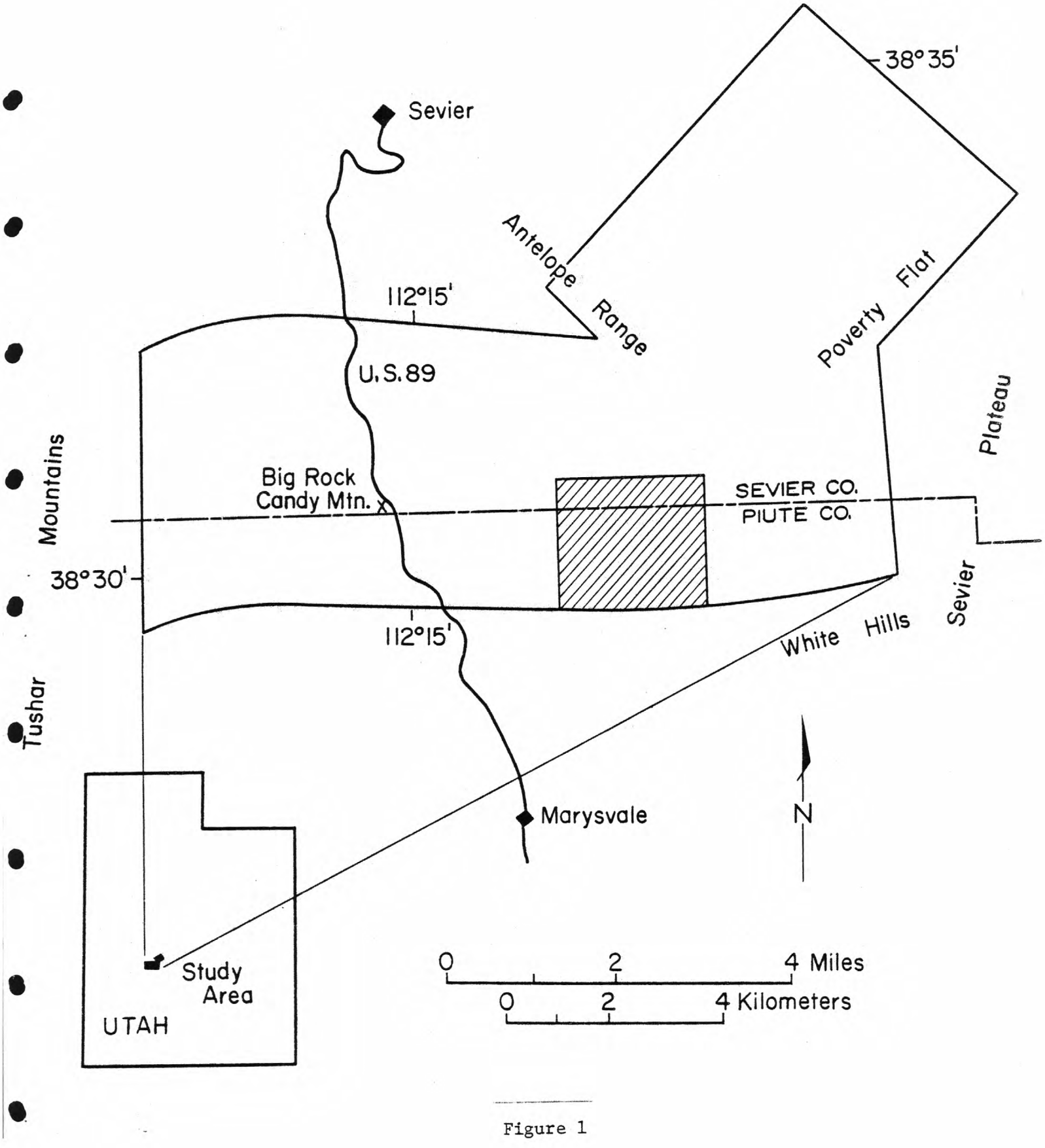
38°35'
Sevier
Antelope Range
Poverty Flat
112°15'
U.S.89
Plateau
Mountains
Big Rock Candy Mtn.
SEVIER CO.
PIUTE CO.
38°30'
112°15'
Sevier
White Hills
Tushar
Marysvale
N
Study Area
UTAH
0 2 4 Miles
0 2 4 Kilometers

Figure 1

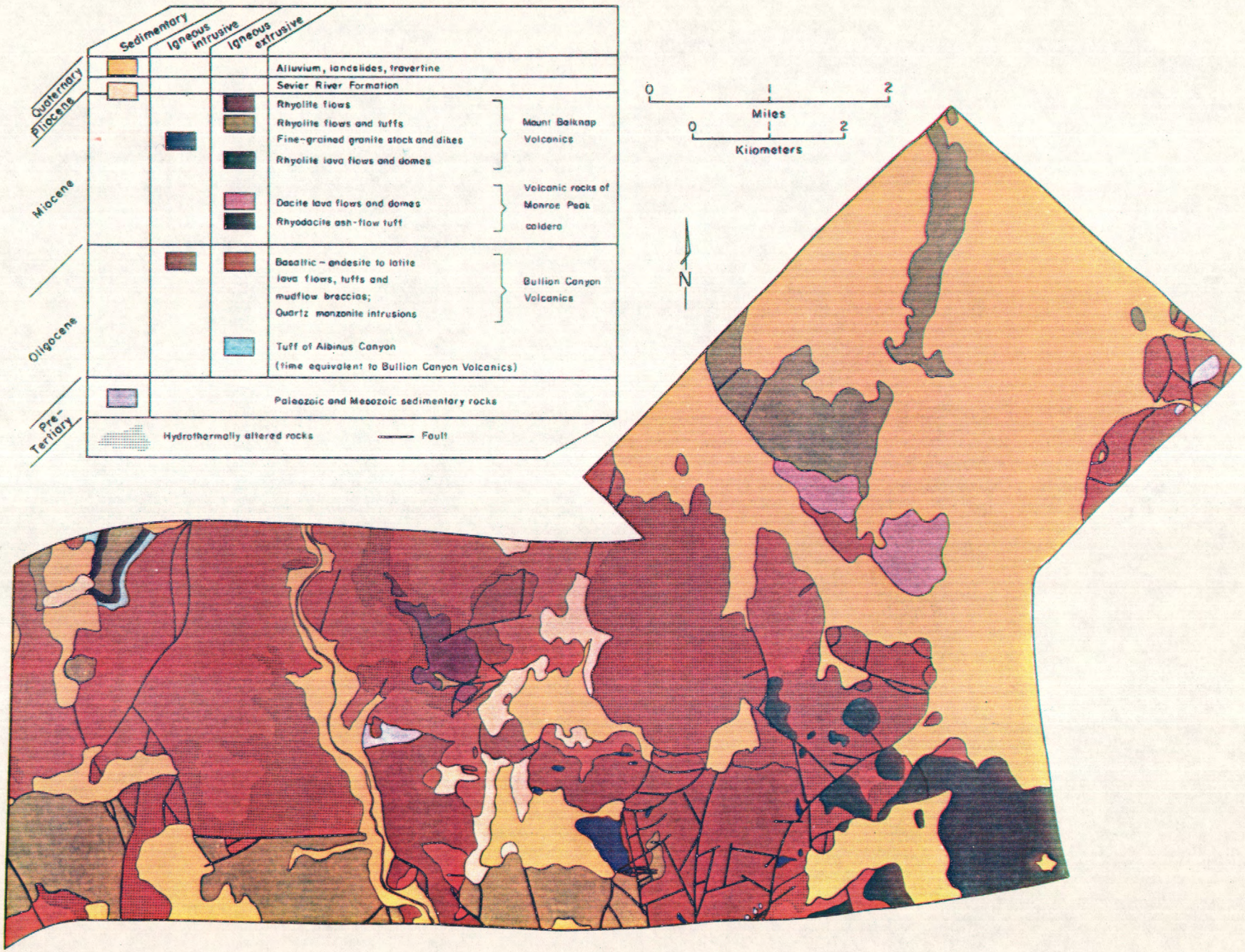
Sedimentary
Igneous intrusive
Igneous extrusive
Quaternary
Pliocene
Miocene
Oligocene
Pre-Tertiary
Alluvium, landslides, travertine
Sevier River Formation
Rhyolite flows
Rhyolite flows and tuffs
Fine-grained granite stock and dikes
Rhyolite lava flows and domes
Mount Belknap Volcanics
Dacite lava flows and domes
Rhyodacite ash-flow tuff
Volcanic rocks of Monroe Peak caldera
Basaltic-andesite to latite lava flows, tuffs and mudflow breccias; Quartz monzonite intrusions
Bullion Canyon Volcanics
Tuff of Albinus Canyon
(time equivalent to Bullion Canyon Volcanics)
Paleozoic and Mesozoic sedimentary rocks
Hydrothermally altered rocks
Fault
0 1 2
Miles
0 1 2
Kilometers
N

Figure 2

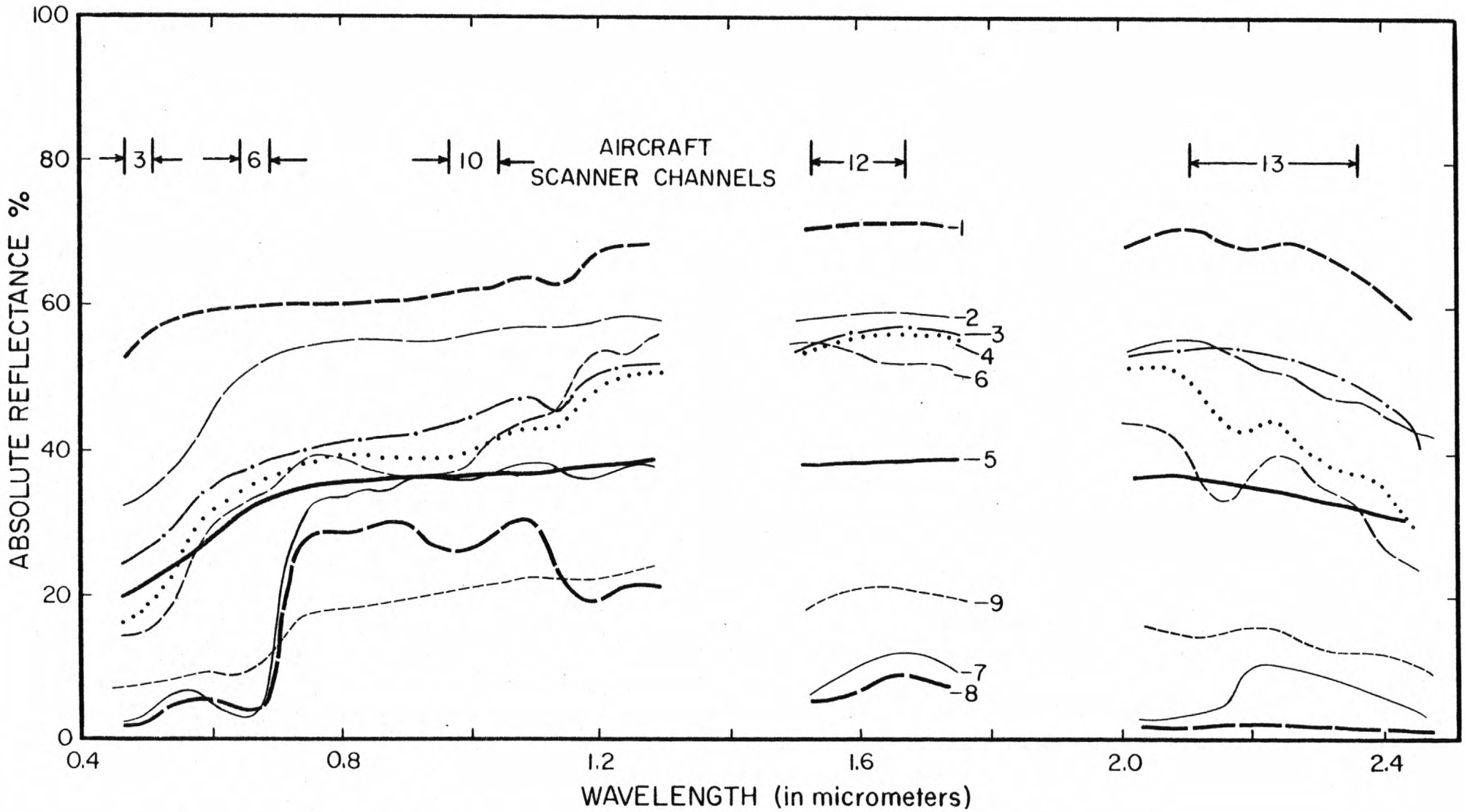

1. White Joe Lott Tuff Member, Mount Belknap Volcanics
2. White zeolite (clinoptilolite)
3. Limonitic Joe Lott Tuff Member, Mount Belknap Volcanics
4. Tan Moenkopi Shale
5. Tan soil on rhyolite
6. Orange altered latite
7. Bigtooth maple
8. Single leaf pinyon pine
9. Big sage

Figure 3

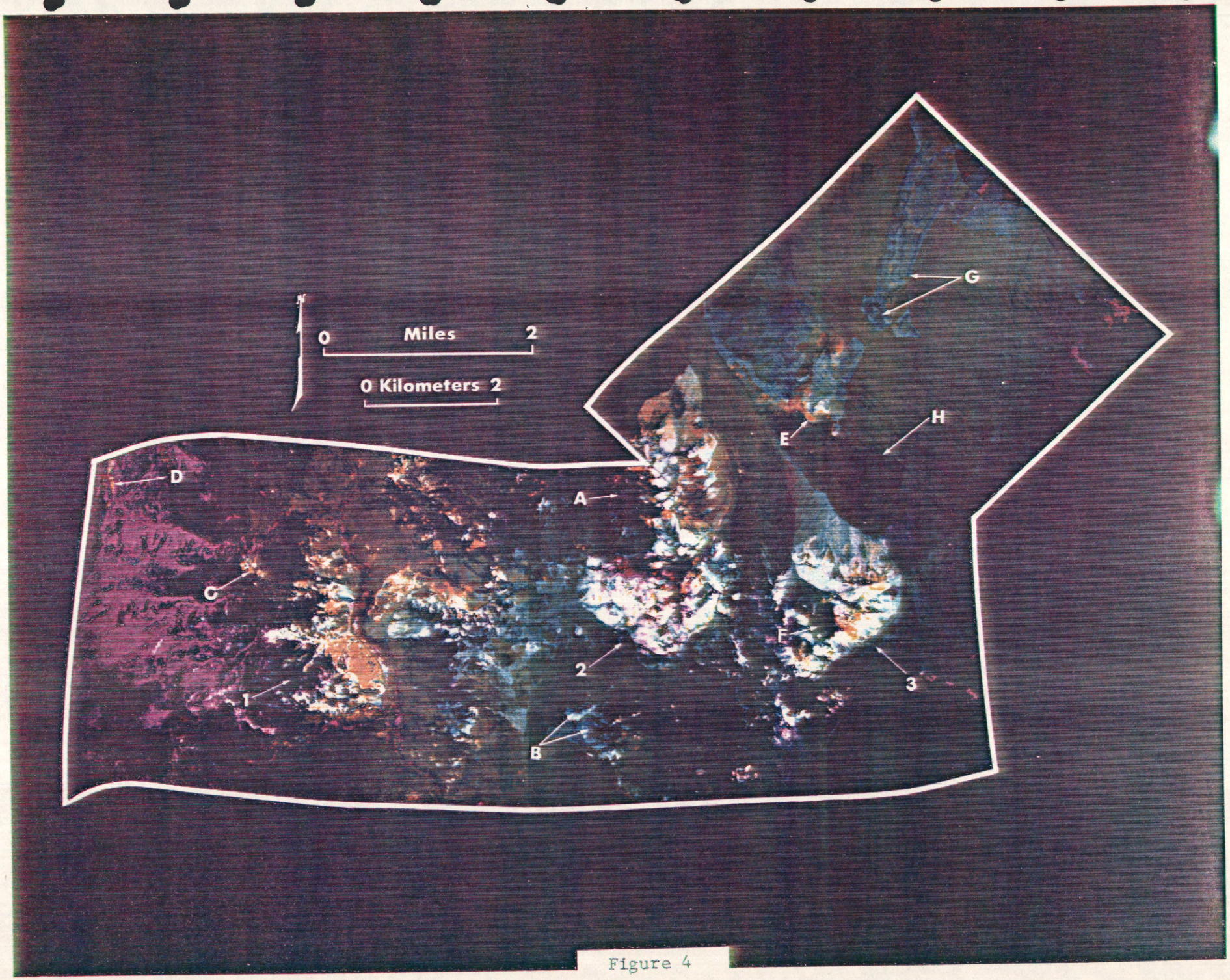

Figure 4

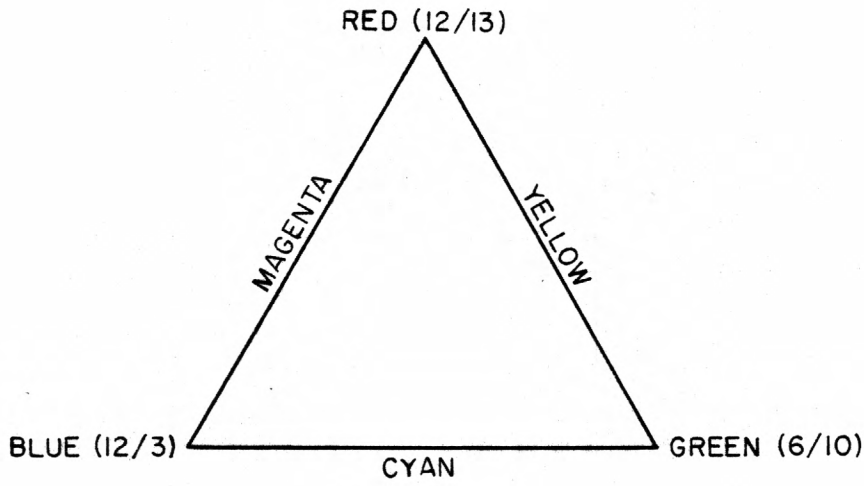

Figure 5

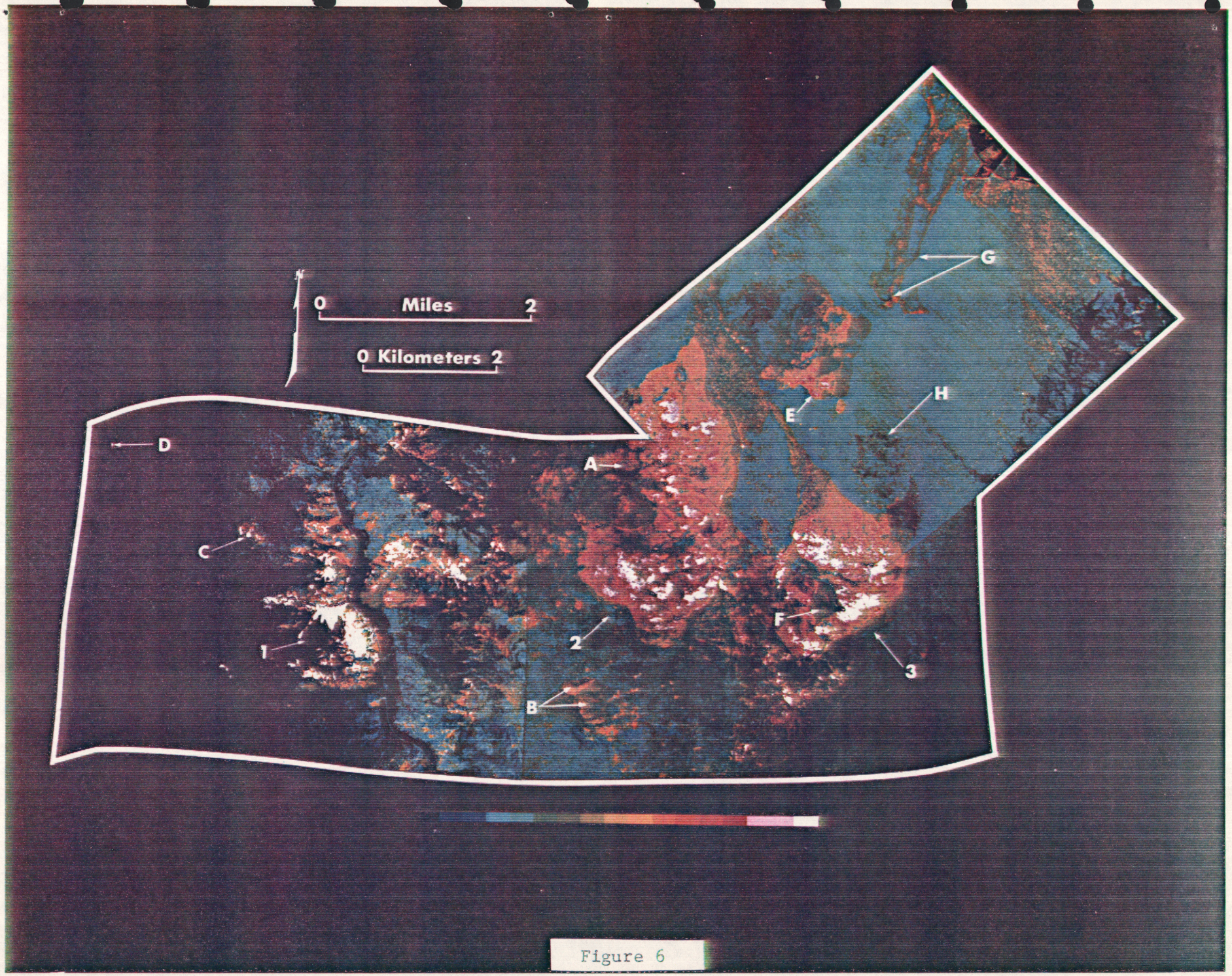

Figure 6

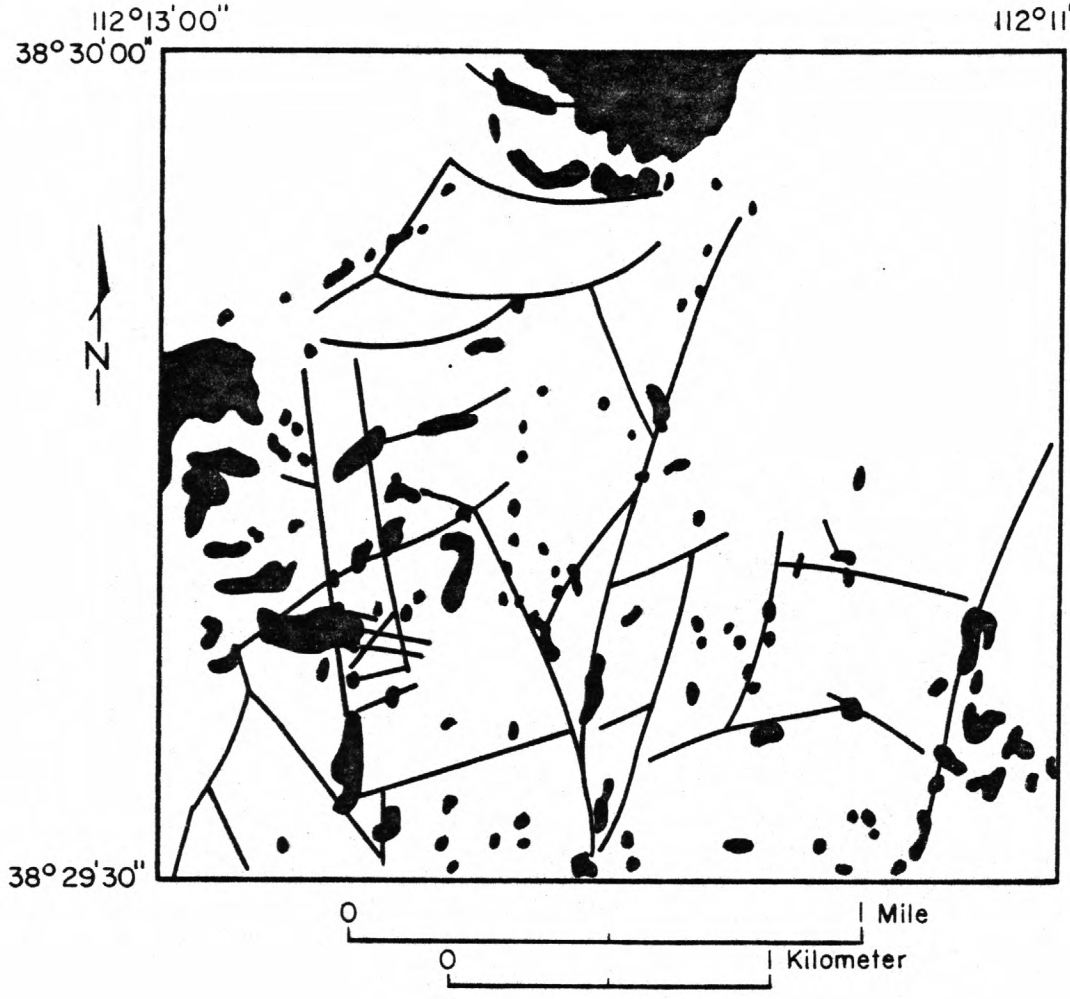

Figure 7